

## Article

# Impact of Binary Chemical Reaction and Activation Energy on Heat and Mass Transfer of Marangoni Driven Boundary Layer Flow of a Non-Newtonian Nanofluid

Ramanahalli Jayadevamurthy Punith Gowda <sup>1</sup>, Rangaswamy Naveen Kumar <sup>1</sup>, Anigere Marikempaiah Jyothi <sup>2</sup>, Ballajja Chandrapa Prasannakumara <sup>1</sup> and Ioannis E. Sarris <sup>3,\*</sup>

<sup>1</sup> Department of Studies and Research in Mathematics, Davangere University, Davangere 577002, Karnataka, India; rpunithgowda@gmail.com (R.J.P.G.); nkrmaths@gmail.com (R.N.K.); dr.bcprasanna@gmail.com (B.C.P.)

<sup>2</sup> Department of Mathematics, Bangalore Institute of Technology, Bangalore 560004, Karnataka, India; jyothijssam05@gmail.com

<sup>3</sup> Department of Mechanical Engineering, University of West Attica, 12244 Athens, Greece

\* Correspondence: sarris@uniwa.gr

**Abstract:** The flow and heat transfer of non-Newtonian nanofluids has an extensive range of applications in oceanography, the cooling of metallic plates, melt-spinning, the movement of biological fluids, heat exchangers technology, coating and suspensions. In view of these applications, we studied the steady Marangoni driven boundary layer flow, heat and mass transfer characteristics of a nanofluid. A non-Newtonian second-grade liquid model is used to deliberate the effect of activation energy on the chemically reactive non-Newtonian nanofluid. By applying suitable similarity transformations, the system of governing equations is transformed into a set of ordinary differential equations. These reduced equations are tackled numerically using the Runge–Kutta–Fehlberg fourth-fifth order (RK45) method. The velocity, concentration, thermal fields and rate of heat transfer are explored for the embedded non-dimensional parameters graphically. Our results revealed that the escalating values of the Marangoni number improve the velocity gradient and reduce the heat transfer. As the values of the porosity parameter increase, the velocity gradient is reduced and the heat transfer is improved. Finally, the Nusselt number is found to decline as the porosity parameter increases.

**Keywords:** second-grade nanofluid; Marangoni convection; chemical reaction; activation energy



**Citation:** Punith Gowda, R.J.; Naveen Kumar, R.; Jyothi, A.M.; Prasannakumara, B.C.; Sarris, I.E. Impact of Binary Chemical Reaction and Activation Energy on Heat and Mass Transfer of Marangoni Driven Boundary Layer Flow of a Non-Newtonian Nanofluid. *Processes* **2021**, *9*, 702. <https://doi.org/10.3390/pr9040702>

Academic Editor: Byeong-Ui Moon

Received: 26 March 2021

Accepted: 14 April 2021

Published: 16 April 2021

**Publisher's Note:** MDPI stays neutral with regard to jurisdictional claims in published maps and institutional affiliations.



**Copyright:** © 2021 by the authors. Licensee MDPI, Basel, Switzerland. This article is an open access article distributed under the terms and conditions of the Creative Commons Attribution (CC BY) license (<https://creativecommons.org/licenses/by/4.0/>).

## 1. Introduction

The study of non-Newtonian liquids is extremely important because of their numerous industrial and engineering usages such as oil reservoir engineering, material processing and foodstuffs. A single relationship cannot be used to classify all non-Newtonian liquids, due to their different features. As a result, different models for describing the properties of non-Newtonian liquids have been proposed. There are three types of non-Newtonian liquid, based on the differential, rate, and integral properties of fluids. The simplest subclass of differential type fluid is the second-grade liquid model. The effect of normal stress is incorporated in this model. However, because of its broad uses in industrial processes like drawing of plastic films, glass fiber, paper production, extrusion of plastic sheets and many others, the study of interface layer flow and heat transfer inducted by stretching surfaces has become interested in non-Newtonian fluids. Motivated by these applications, several investigators have examined the flow of second-grade nanofluids past stretchy sheets. Hayat et al. [1] considered the Newtonian heating effect on second-grade liquid flow above a stretchy sheet. Javanmard et al. [2] studied the magnetohydrodynamic (MHD) flow of second-grade liquid above a stretch sheet. Hayat et al. [3] explicated the induced magnetic field impact on the second-grade fluid stream with suspended nanoparticles above a stretchy surface. Krishna et al. [4] elucidated the second-grade fluid flow above an elastic

sheet. Kalaivanan et al. [5] elucidated aspects of activation energy on the second-grade fluid flow with suspended nanoparticles above a stretchy sheet.

The nanofluid is a combination of nanoparticles and a carrier liquid. The base fluid is usually a conductive fluid, such as oil, water or ethylene glycol, and the nanoparticles are usually made of metals or non-metals. The solid metals have a greater thermal conductivity than base fluids. Due to this, suspended nanoparticles can improve thermal conductivity and heat transference performance. Nanofluids are used in a variety of engineering and technical applications, including vehicle thermal management, vehicle cooling, heat exchangers, nuclear reactors, electronic device cooling, etc. The concept of nanofluids was initially introduced by Choi [6]. Recently, Radhika et al. [7] considered dusty liquid flow with a dual nanoparticle suspension over a stretchy sheet with a melting effect. Shafiq et al. [8] studied the chemically reacting bioconvective stream of second-grade liquid with a nanoparticle suspension above a stretchy geometry. Shah et al. [9] explicated the flow of second-grade liquid with carbon nanotubes above a stretchy sheet and discussed the entropy production. Gowda et al. [10] studied the stream of liquid with a hybrid nanoparticles suspension over a moving disk with spin by considering particle deposition.

In 1889, Svante Arrhenius coined the term “Arrhenius activation”. It is the minimal energy that a chemical system with potential reactants would need in order to achieve a chemical reaction. A reaction happens when the atoms move quickly due to the activation energy. In the chemistry world, activation energy is very important. Arrhenius activation energy occurs in many chemically reacting systems, with examples in oil reservoir and geothermal engineering. Initially, the concept of binary chemical reaction was introduced by Bestman [11]. Recently, Khan et al. [12] discussed the aspects of binary chemical reaction on nanofluid flow past a surface with activation energy. Jayadevamurthy et al. [13] studied the bioconvective flow of a hybrid nanofluid above a moving disk with activation energy. Reddy et al. [14] explored aspects of activation energy with chemical reaction on the MHD flow of hybrid nanofluid. Zhao et al. [15] experimentally analyzed the chemical reaction monitoring via the light focusing in optofluidic waveguides.

The Marangoni convection phenomenon has piqued the interest of scholars and scientists because of its global applications. Marangoni convection is initiated by changes in surface tension gradients. Marangoni boundary layers may form at liquid–liquid interfaces. The Marangoni convection phenomenon is widely used in artworks like ground dyeing. A dye or pigment is floated on top of the basic medium in this technique. Additionally, it has applications in crystal growth, welding, soap film stabilization, silicon wafer drying and obligatory convection. Recently, Rasool et al. [16] investigated the Marangoni effect on the flow of second-grade nanofluid above a stretchy geometry. Khan et al. [17] studied the Marangoni convective flow of second-grade liquid above a stretchy sheet. Hayat et al. [18] demonstrated the aspects of chemical reaction on the Marangoni convective flow of second-grade liquid. Ullah et al. [19] explored the chemically reactive flow of a nanoliquid with activation energy. Qayyum [20] studied the Marangoni convective stream of hybrid nanofluid above a stretchy surface.

From the aforementioned articles, to the best of the author’s knowledge, second-grade liquid flow over a surface with Marangoni convection and nanoparticles suspension has not yet been discussed. Non-Newtonian fluids, when compared with Newtonian liquids, are considered to be more suitable fluid models in technological and industrial applications because of their applications in welding, beam melting and crystal growth mechanisms. Numerous researchers are currently involved in finding numerical or analytical solutions for flow problems that arise by means of diverse non-Newtonian liquids. The flow analysis is more complex and subtler when compared with Newtonian fluids, due to the non-linear dependence of stresses on the rate of strain for non-Newtonian fluids. Additionally, the Marangoni convection appears in many applications in industrial, biomedical and daily life such as surfactant replacement therapy for neonatal infants, coating flow technology, foams, microfluidics and film drainage in emulsions. Hence, the key role of this study is to

inspect the Marangoni driven boundary layer flow, heat and mass transfer characteristics of a non-Newtonian nanofluid with activation energy and binary chemical reactions.

## 2. Mathematical Formulation

Consider a rectangular coordinate system in which  $x$  and  $y$  are measured along the surface and perpendicular to the surface, respectively, and flow is confined at half plane  $y \geq 0$ , as shown in Figure 1. Moreover, the spatial variation in surface tension is characterized by a gradient in temperature and solute concentration. The nanofluid consists of a sample liquid (engine oil) along with suspended  $TC_4$  (Ti-6Al-4 V) nanoparticles. The surface tension  $\sigma = \sigma_0[1 - \gamma_T(T - T_\infty) - \gamma_C(C - C_\infty)]$  is supposed to depend on linear fluctuation with temperature and concentration boundaries, where the surface tension coefficients for temperature is  $\gamma_T = -\frac{1}{\sigma_0} \frac{\partial \sigma}{\partial T} \Big|_T$  and concentration is  $\gamma_C = -\frac{1}{\sigma_0} \frac{\partial \sigma}{\partial C} \Big|_C$ .

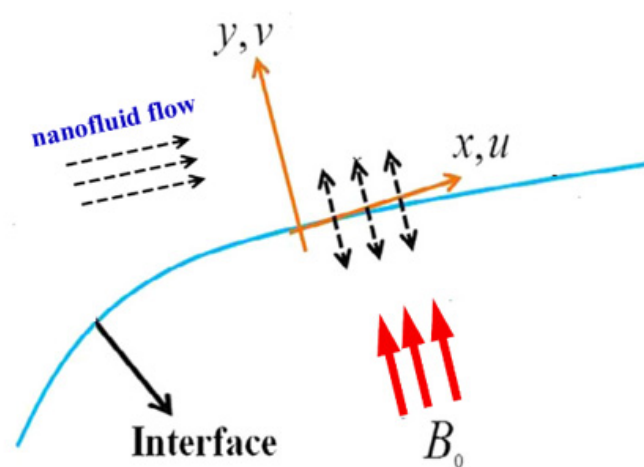


Figure 1. Flow description.

### 2.1. Conditions and Assumptions of the Model

The mathematical model is considered under the following assumptions and conditions:

- Two-dimensional laminar flow;
- Porous medium;
- Marangoni convection;
- Second-grade nanofluid;
- Binary chemical reaction with activation energy.

### 2.2. Flow Geometry

We illustrate the flow geometry of the model as follows.

### 2.3. Model Equations

Under these assumptions, the modelled equations are put into the following arrangement [16,17,21]:

$$\frac{\partial u}{\partial x} + \frac{\partial v}{\partial y} = 0, \quad (1)$$

$$u \frac{\partial u}{\partial x} + v \frac{\partial u}{\partial y} = \nu_{nf} \frac{\partial^2 u}{\partial y^2} + \frac{\alpha_1}{\rho_{nf}} \left( \frac{\partial u}{\partial x} \frac{\partial^2 u}{\partial y^2} + u \frac{\partial^3 u}{\partial y^2 \partial x} - \frac{\partial u}{\partial y} \frac{\partial^2 u}{\partial y \partial x} + v \frac{\partial^3 u}{\partial y^3} \right) - \frac{\nu_{nf}}{K^*} u - \frac{\sigma_1 B_0^2}{\rho_{nf}} u, \quad (2)$$

$$u \frac{\partial T}{\partial x} + v \frac{\partial T}{\partial y} = \frac{k_{nf}}{(\rho C_p)_{nf}} \left( \frac{\partial^2 T}{\partial y^2} \right) + \frac{Q}{(\rho C_p)_{nf}} (T - T_\infty) - \frac{1}{(\rho C_p)_{nf}} \frac{\partial q_r}{\partial y}, \quad (3)$$

$$u \frac{\partial C}{\partial x} + v \frac{\partial C}{\partial y} = D_{nf} \frac{\partial^2 C}{\partial y^2} - k_r^2 (C - C_\infty) \left( \frac{T}{T_\infty} \right)^m \exp \left( -\frac{E_a}{k^* T} \right). \quad (4)$$

The relative boundary constraints are itemized as

$$y = 0 : \mu_{nf} \frac{\partial u}{\partial y} = -\frac{\partial \sigma}{\partial x} = \sigma_0 \left( \gamma_T \frac{\partial T}{\partial x} + \gamma_C \frac{\partial C}{\partial x} \right), v = 0, T = T_\infty + T_0 X^2, C = C_\infty + C_0 X^2, \left. \vphantom{\frac{\partial u}{\partial y}} \right\} \quad (5)$$

$$y \rightarrow \infty : u \rightarrow 0, \frac{\partial u}{\partial y} \rightarrow 0, T \rightarrow T_\infty, C \rightarrow C_\infty.$$

The following similarity transformation procedure is employed

$$\left. \begin{aligned} \psi &= v_f X f(\eta), \eta = \frac{y}{L}, X = \frac{x}{L}, \\ u &= \frac{\partial \psi}{\partial y}, v = -\frac{\partial \psi}{\partial x}, \\ T &= T_\infty + T_0 X^2 \theta(\eta), C = C_\infty + C_0 X^2 \chi(\eta). \end{aligned} \right\} \quad (6)$$

where  $(u, v)$  ( $\text{ms}^{-1}$ ) are the velocity components in the direction of  $(x, y)$  (m).  $L$  (m) is the reference length,  $\mu$  ( $\text{kg s}^{-1} \text{m}^{-1}$ ) is the dynamic viscosity, thermal conductivity is given by  $k$ ,  $D$  ( $\text{m}^2 \text{s}^{-1}$ ) represents diffusivity coefficient,  $T$  (K) and  $C$  are the temperature and concentration of the liquid, respectively,  $C_p$  ( $\text{K}^{-1} \text{s}^{-2} \text{m}^2$ ) is the heat capacity,  $K^*$  ( $\text{m}^2$ ) is the porous medium permeability,  $\alpha_1$  is the second-grade material-related parameter,  $\nu$  ( $\text{m}^2 \text{s}^{-1}$ ) is the kinematic viscosity,  $\sigma_1$  ( $\text{kg}^{-1} \text{m}^{-3} \text{c}^2 \text{s}$ ) is the electrical conductivity,  $B_0$  ( $\text{kg}^{1/2} \Omega^{1/2} \text{s}^{-1/2} \text{m}^{-1}$ ) is the magnetic field,  $\rho C_p$  ( $\text{kg m}^{-1} \text{s}^{-2} \text{K}^{-1}$ ) is the specific heat capacity,  $Q$  is the heat source/sink co-efficient,  $k_r^2$  ( $\text{s}^{-1}$ ) is the reaction rate,  $k^*$  is the Boltzmann constant,  $E_a$  is the activation energy,  $m$  is the fitted rate constant,  $\sigma$  is the surface tension, and  $\sigma_0$  is the surface tension at the boundary.

#### 2.4. Rosseland Approximation

The radiative heat flux in terms of Rosseland approximation for linear thermal radiation is given by [22]:

$$q_r = \frac{-4\sigma^{**}}{3k^*} \frac{\partial T^4}{\partial y} \quad (7)$$

Here, we express,  $T^4 = 4T_\infty^3 T - 3T_\infty^4$  as a linear function of temperature.

Now, Equation (3) can be written using Equation (7), as follows:

$$u \frac{\partial T}{\partial x} + v \frac{\partial T}{\partial y} = \left[ \frac{k_{nf}}{(\rho C_p)_{nf}} + \frac{16\sigma^{**}}{(\rho C_p)_{nf} 3k^*} T_\infty^3 \right] \frac{\partial^2 T}{\partial y^2} + \frac{Q}{(\rho C_p)_{nf}} (T - T_\infty), \quad (8)$$

#### 2.5. Thermophysical Features of the Second Grade-Nanofluid

The dispersion of nanoparticles into engine oil fluid causes enhanced thermophysical features. The effective density, heat capacitance, dynamic viscosity, thermal conductivity and diffusivity of the nanofluids are defined as follows [23].

$$\rho_{nf} = \rho_f \left[ (1 - \phi) + \frac{\rho_s}{\rho_f} \phi \right] \quad (9)$$

$$(\rho C_p)_{nf} = (\rho C_p)_f \left[ (1 - \phi) + \frac{(\rho C_p)_s}{(\rho C_p)_f} \phi \right] \quad (10)$$

$$(1 - \phi)^{2.5} \mu_{nf} = \mu_f \quad (11)$$

$$\frac{k_{nf}}{k_f} = \frac{(k_s + 2k_f) - 2\phi(k_f - k_s)}{(k_s + 2k_f) + \phi(k_f - k_s)}, \quad (12)$$

$$D_{nf} = D_f (1 - \phi)^{2.5}. \quad (13)$$

where  $(\rho C_p)_f$ ,  $(\rho C_p)_s$ ,  $\rho_f$ ,  $\rho_s$ ,  $k_f$  and  $k_s$  are the specific heat capacity, density and thermal conductivity of the base fluid and a particle, respectively.  $\rho_{nf}$ ,  $(\rho C_p)_{nf}$ ,  $\mu_{nf}$ ,  $k_{nf}$  and  $D_{nf}$  are

the density, specific heat capacity, dynamic viscosity, thermal conductivity and diffusion co-efficient of nanofluid, respectively;  $\phi$  is the solid volume fraction,  $\mu_f$  is the dynamic viscosity of the base fluid and  $D_f$  is the diffusion co-efficient of base liquid.

### 2.6. Nanoparticles and Base Fluid Features

Table 1 shows the material properties of the base liquid and nanoparticle used in this study [24].

**Table 1.** The thermophysical properties of base fluid and nanoparticles.

Physical Properties	$C_p$ (J/kgK)	$k$ (W/mK)	$\rho$ (kg/m <sup>3</sup> )
Engine Oil (Unused 360 K)	2126	0.138	847.8
TC <sub>4</sub>	610	5.8	4420

### 3. The Solution for the Problem

The reduced non-dimensional form of mathematical equations is as follows

$$\varepsilon_1 f''' - [f'^2 - ff''] + \alpha_2 \varepsilon_2 [2f'f''' - f''^2 - ff^{iv}] - \varepsilon_1 \lambda^* f' - \varepsilon_2 M f' = 0, \quad (14)$$

$$\varepsilon_3 \frac{1}{Pr} \left( \frac{k_{nf}}{k_f} + R_d \right) \theta'' - [2f'\theta - f\theta'] + \varepsilon_3 Q_0 \theta = 0, \quad (15)$$

$$\varepsilon_4 \frac{1}{Sc} \chi'' - [2f'\chi - f\chi'] - \sigma^* (1 + \delta\theta)^m \exp\left(\frac{-E}{(1 + \delta\theta)}\right) \chi = 0, \quad (16)$$

where

$$\varepsilon_1 = \frac{1}{(1 - \phi)^{2.5} \left[ 1 - \phi + \phi \frac{\rho_s}{\rho_f} \right]}, \quad \varepsilon_2 = \frac{1}{\left[ 1 - \phi + \phi \frac{\rho_s}{\rho_f} \right]},$$

$$\varepsilon_3 = \frac{1}{\left[ 1 - \phi + \phi \frac{(\rho C_p)_s}{(\rho C_p)_f} \right]}, \quad \varepsilon_4 = (1 - \phi)^{2.5}.$$

The transformed boundary conditions are

$$\left. \begin{aligned} f''(0) &= -2(1 - \phi)^{2.5}(1 + Ma), f(0) = 0, \theta(0) = 1, \chi(0) = 1, \\ f'(\infty) &\rightarrow 0, f''(\infty) \rightarrow 0, \theta(\infty) \rightarrow 0, \chi(\infty) \rightarrow 0. \end{aligned} \right\} \quad (17)$$

#### 3.1. Expression of Parameters

$\alpha_2 = \frac{\alpha_1}{\rho_f L^2}$  is the second-grade fluid parameter,  $\lambda^* = \frac{L^2}{K^*}$  is the porosity parameter,  $Pr = \frac{\nu_f (\rho C_p)_f}{k_f}$  is the Prandtl number,  $Sc = \frac{\nu_f}{D_f}$  is the Schmidt number,  $E = \frac{E_a}{k^* T_\infty}$  is the non-dimensional activation energy,  $\sigma^* = \frac{k_f^2 L^2}{\nu_f}$  is the chemical reaction rate parameter,  $M = \frac{\sigma_1 B_0^2 L^2}{\mu_f}$  is the magnetic parameter,  $Q_0 = \frac{QL^2}{(\rho C_p)_f \nu_f}$  is the heat source/sink parameter,  $\delta = \frac{T_0 X^2}{T_\infty}$  is the temperature difference,  $Ma = \frac{C_0 \gamma_C}{T_0 \gamma_T}$  is the Marangoni number and  $R_d = \frac{16\sigma^* T_\infty^3}{3k^* k_f}$  is the radiation parameter.

### 3.2. Physical Quantities of Engineering Interests

Typical measurement of engineering physical interest quantity, which gives the rate of heat transfer at the surface is as follows:  $Nu_x = -\frac{xk_{nf} \frac{\partial T}{\partial y} \Big|_{y=0} + (q_r)_w}{k_f(T-T_\infty)}$ , and its non-dimensional form is given by

$$Nu_x = -\left(\frac{k_{nf}}{k_f} + R_d\right)\theta'(0). \quad (18)$$

### 4. Numerical Method

Obtaining the exact solution of the current model, which is highly non-linear in nature, does not seem to be feasible. Hence, by using an interactive environment and high-level language, these equations are solved numerically using the RKF-45 technique. To handle the end-point singularities, a sub method called the midpoint method is considered with the Richardson extrapolation enhancement scheme. The ODEs Equations (9)–(11) are converted into the system of first-order differential equations (Equations (19)–(26)) by using the substitutions  $f = y_1, f' = y_2, f'' = y_3, f''' = y_4, \theta = y_5, \theta' = y_6, \chi = y_7, \chi' = y_8$  as follows

$$y'_1 = y_2, \quad (19)$$

$$y'_2 = y_3, \quad (20)$$

$$y'_3 = y_4, \quad (21)$$

$$y'_4 = \frac{\varepsilon_1 y_4 - [y_2^2 - y_1 y_3] + \alpha_2 \varepsilon_2 [2y_2 y_4 - y_3^2] - \varepsilon_1 \lambda^* y_2 - \varepsilon_2 M y_2}{\alpha_2 \varepsilon_2 y_1}, \quad (22)$$

$$y'_5 = y_6, \quad (23)$$

$$y'_6 = \frac{Pr([2y_2 y_5 - y_1 y_6] - \varepsilon_3 Q_0 y_5)}{\varepsilon_3 \left(\frac{k_{nf}}{k_f} + R_d\right)}, \quad (24)$$

$$y'_7 = y_8, \quad (25)$$

$$y'_8 = \frac{Sc([2y_2 y_7 - y_1 y_8] + \sigma^*(1 + \delta y_5)^m \exp\left(\frac{-E}{(1+\delta y_5)}\right) y_7)}{\varepsilon_4}, \quad (26)$$

along with the boundary conditions Equation (12), as

$$\left. \begin{aligned} y_3(0) &= -2(1 - \phi)^{2.5}(1 + Ma), y_1(0) = 0, y_5(0) = 1, y_7(0) = 1, \\ y_2(\infty) &\rightarrow 0, y_3(\infty) \rightarrow 0, y_5(\infty) \rightarrow 0, y_7(\infty) \rightarrow 0, \end{aligned} \right\} \quad (27)$$

Unspecified initial conditions are handpicked and the calculations are carried out systematically for several values of formerly defined parameters.

It is important to note that convergence is not ensured, particularly if missing initial values are predicted incorrectly. When one of the domain end-points is at infinity, another struggle occurs due to the inconsistency of boundary value problems. Hence, the vital step of this method is to pick the apt finite value of  $\eta_\infty$ . To satisfy far-field boundary conditions asymptotically, we select an apt finite value of  $\eta_\infty$ . Mesh selection and error management are based on the rest of the ongoing solution. The step size selected as  $\Delta\eta = 0.0001$ , along with the comparative error tolerance as  $10^{-6}$ , which is well-organized for convergence criteria. The CPU time to guess the velocity values (1.42 s) is much shorter when compared to the CPU time required to estimate the concentration (2.21 s) and thermal values (1.56 s). This technique's validity is verified by comparing the results of the current method's heat transference rate with those found in the literature [25–29].

## 5. Result and Discussion

The influence of Marangoni convection on a second-grade nanoliquid stream over a surface with porous medium is deliberated in this study. Further, a non-Newtonian nanoliquid suspended with  $TC_4$  as nanoparticles in base fluid engine oil is considered in this modelling. The primary goal of the current segment is to study the impact of several dimensionless variables on velocity, temperature and concentration profiles. It is worth noting that the equations governing the assumed flow are reduced to ODEs by selecting appropriate similarity variables. The RKF-45 method is used to perform two-dimensional simulations for non-linear coupled systems. In the presence of a porous medium in a surface-tension driven convection, the figured results are expressed. To calculate the most accurate results, the suitable initial guesses and several values of dimensionless parameters must be carefully selected and well-adjusted. The Prandtl number is set as fixed in this analysis, while the other parameters are varied to investigate their effects on stream, mass and heat transfer. The solutions are introduced to show the impact of many important parameters on velocity, concentration and thermal gradients. Table 2 represents the comparative study of current work with published articles and they are found to be in agreement with each other.

**Table 2.** A comparison of the  $-\theta'(0)$  with published results for different values of  $Pr$ .

$Pr$	0.72	1	3	10
Mabood and Shateyi [25]	0.8088	1.0000	1.9237	3.7207
Dulal Pal [26]	-	1.0000	1.9236	3.7207
Haile and Shankar [27]		1.0004	1.9234	3.7205
Ishak et al. [28] (Exact solution)	0.8086313498	1.000000000	1.923682594	3.720673901
Ali et al. [29] (FEM solution)	0.8086339289	1.0000080210	1.9236777223	3.7206681685
Current results	0.8086332536	1.0000062839	1.9236749758	3.7206678659

The impact of  $M$  on  $f'(\eta)$  is depicted in Figure 2. Here, the rising values of  $M$  reduce the  $f'(\eta)$ . The importance of the magnetic field on the flow field is represented by  $M$ . The occurrence of a magnetic field in the flow field area slows down the fluid motion. The ratio of viscous force and magnetic force gives the magnetic parameter. Physically, it arises due to the Lorentz force, which creates more struggle to the fluid motion. The Lorentz force comes from the magnetic field, which acts as a delaying force. As seen in Figure 2, this negative body force slows the boundary layer flow and opposes momentum diffusion, which leads to the lessening of velocity. The influence of  $M$  on  $\theta(\eta)$  is portrayed in Figure 3. Here, the rising values of  $M$  improve  $\theta(\eta)$ . These findings suggest that the magnetization force adds a layer of resistance to the flow, lowering the velocity and increasing the temperature. Lorentz force is induced by the presence of a transverse magnetic field, resulting in a retarding force on nanoparticles and the base fluid velocity field. Thermal energy is dissipated as a result of the additional work required to pull the nanofluid toward the magnetic field's operation. This warms the nanofluid, which raises the temperature of the fluid. As the value of  $M$  increases, the retarding force increases and the thermal gradient decreases as a result of this intervention in the flow. In general, the presence of an electromagnetic field significantly improves the heat passage mechanism.

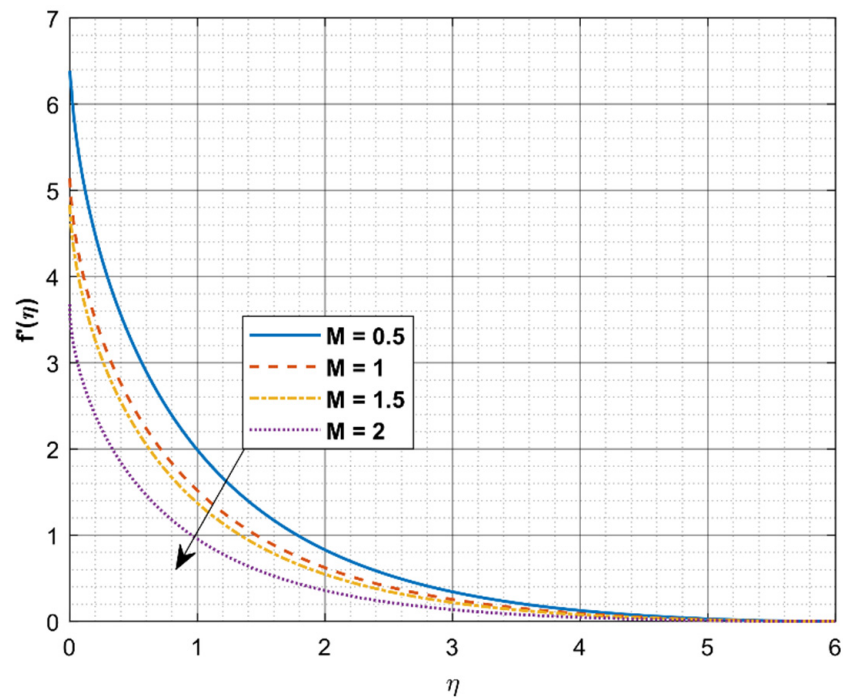


Figure 2. Influence of  $M$  on  $f'(\eta)$ .

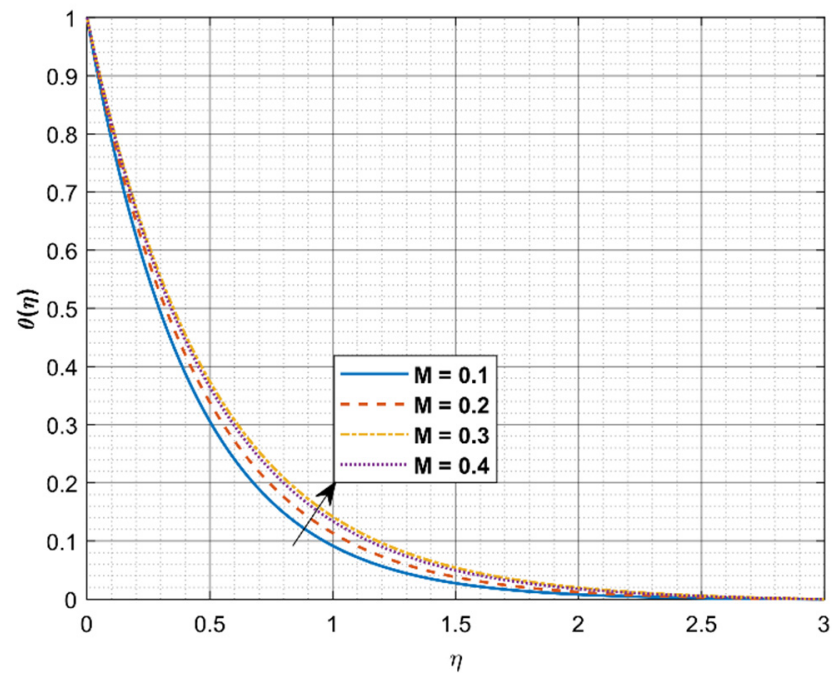


Figure 3. Influence of  $M$  on  $\theta(\eta)$ .

The influence of  $\lambda^*$  on  $f'(\eta)$  is illustrated in Figure 4. Here, as  $\lambda^*$  values are increased, the velocity gradient declines. Physically, the increase in  $\lambda^*$  is due to the reduction in the mean absorption coefficient and the resistive power used by the permeable region, which cause the velocity gradient to decline. The liquid has more space to flow when the porousness is massive than is when it is decreasing. As a result, the velocity increases. Closer to the surface, however, the change in velocity is greatest, while, farther away, the change is minimal. The effect of  $\lambda^*$  on  $\theta(\eta)$  is demonstrated in Figure 5. As  $\lambda^*$  increases, the fluid's temperature increases as well. Here, fluid becomes more viscous with the increase in  $\lambda^*$ , and the fluid's velocity stagnates as a result of the increased viscosity. Since it limits

fluid motion along the surface, the  $\lambda^*$  reflects resistance to movement with an increase in thermal gradient. This is in line with the fact that increasing  $\lambda^*$  adds some extra tension which is accountable for the thermal boundary layer thickening.

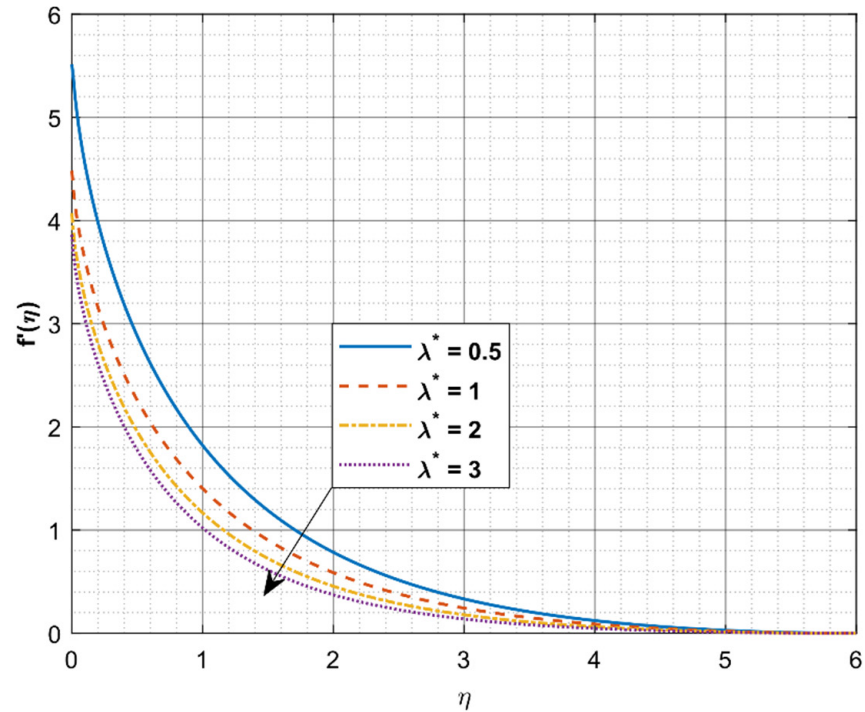


Figure 4. Influence of  $\lambda^*$  on  $f'(\eta)$ .

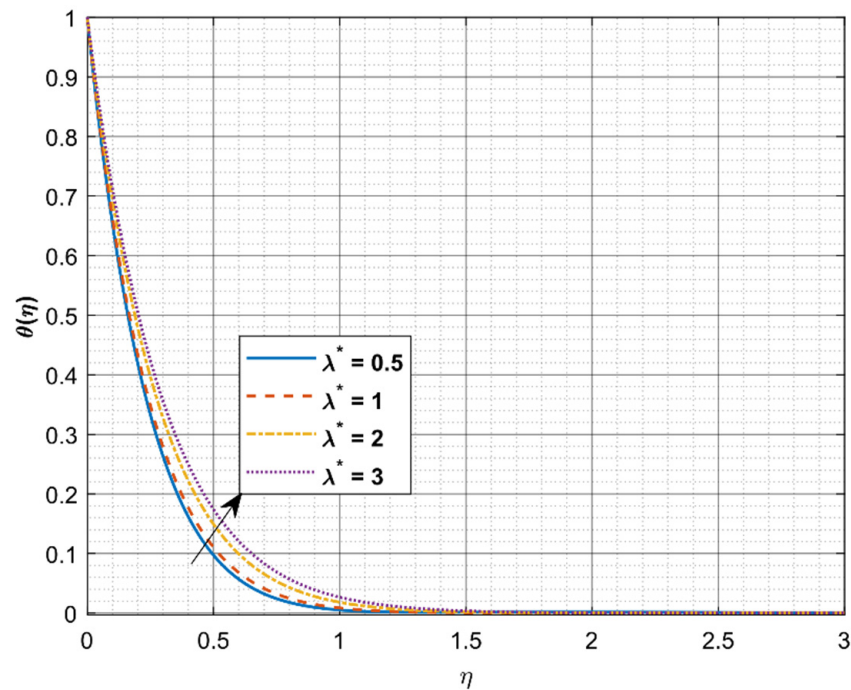


Figure 5. Influence of  $\lambda^*$  on  $\theta(\eta)$ .

The leveraging of  $Ma$  on  $f'(\eta)$  is shown in Figure 6. The graphed figure reveals that increasing the values of  $Ma$  improves the velocity gradient. This behavior is due to the variation in surface tension. Meanwhile, the Marangoni effect is a pouring force for liquid

stream, a stronger Marangoni effect would almost inevitably increase the velocity gradient. Figure 7 depicts the influence of  $Ma$  on  $\theta(\eta)$ . The upsurge in values of  $Ma$  decays the thermal gradient. The Marangoni number is physically tied to the surface tension. Surface tension is the tension in a liquid's surface film caused by the bulk attraction of the liquid to the particles in the surface layer, which helps to limit surface area. Hence, as surface tension increases, temperature decreases and a strong attraction between surface molecules develops. As a result, the thermal gradient deteriorates.

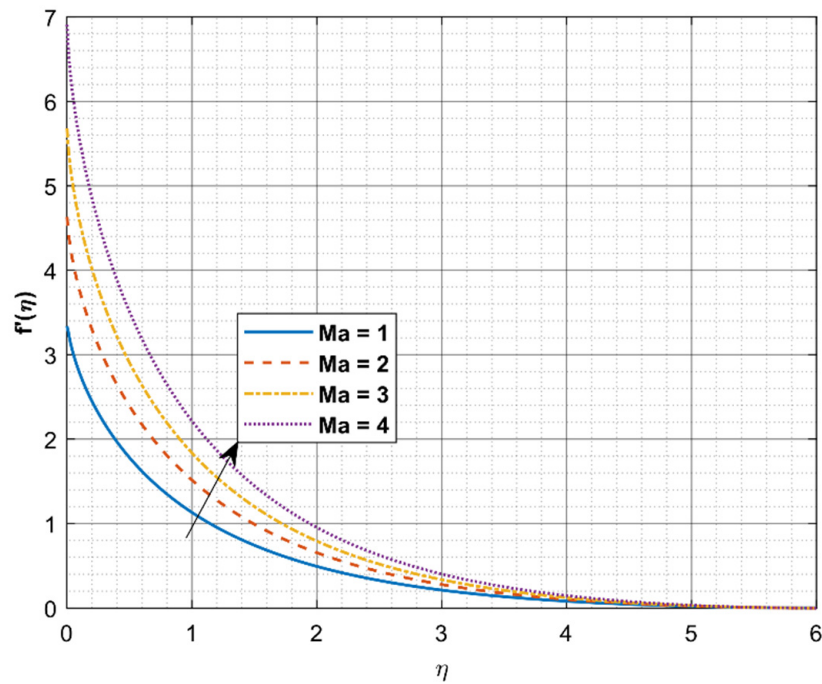


Figure 6. Influence of  $Ma$  on  $f'(\eta)$ .

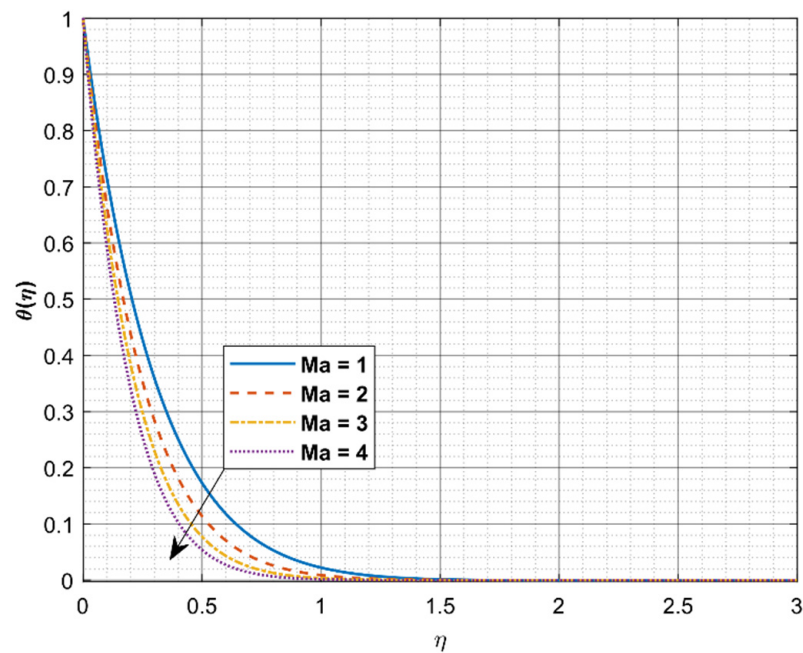


Figure 7. Influence of  $Ma$  on  $\theta(\eta)$ .

The influence of  $Q_0$  on  $\theta(\eta)$  is described in Figure 8. Here, the rising values of  $Q_0$  improve  $\theta(\eta)$ . The term  $Q(T - T_\infty)$  refers to the amount of heat produced/consumed per unit volume; internal heat generation/absorption actually improves or dampens heat transfer. An increase in  $Q_0$  increases the thickness of the thermal boundary layer, mechanically revealing the fact that increasing the heat source's intensity corresponds to a greater thermal diffusion layer, which may increase the thickness of the thermal boundary layer. Here, the presence of the heat source limits in the flow state produces more heat. Due to the production of energy in the thermal boundary layer, an upsurge in  $Q_0$  causes a growth in the temperature profile in the thermal boundary layer regime, as seen in Figure 8. The presence of a heat source energizes the nanofluid. As a result, the buoyancy force accelerates the flow when heat is consumed.

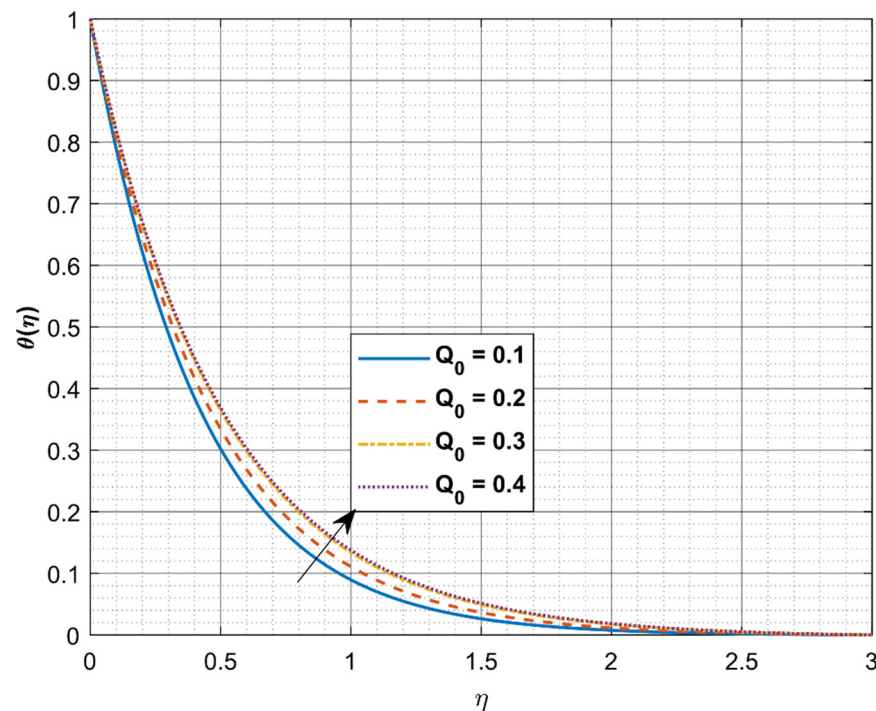


Figure 8. Influence of  $Q_0$  on  $\theta(\eta)$ .

The influence of  $R_d$  on  $\theta(\eta)$  is portrayed in Figure 9. Here, the rising values of  $R_d$  improve  $\theta(\eta)$ . Physically, this is because of the decrease in mean absorption coefficient due to higher values of  $R_d$ . The radiative heat transfer is less efficient than a conductive heat transfer, which lowers the buoyancy force. High  $R_d$  effectively delivers more heat to usable nanofluids, resulting in an increase in  $\theta(\eta)$ . When  $R_d$  is at a lower value, the change is more incremental. When the radiation parameter is set to a high value, the fluid is heated more and more. As a result, an increase in the temperature profile is noticed.

The impact of  $Sc$  on mass transfer is portrayed in Figure 10. The increase in the values of  $Sc$  deteriorates the concentration gradient. The Schmidt number is a dimensionless number that describes the relationship between mass diffusivity and momentum diffusivity in a fluid flow. The maximum concentration of nanoparticles corresponds to the smallest  $Sc$ . It also shows the thickness of the hydrodynamic and nanoparticle species boundary layers. The decay in concentration field is due to mass diffusion which occurs due to an enrichment in the  $Sc$ .

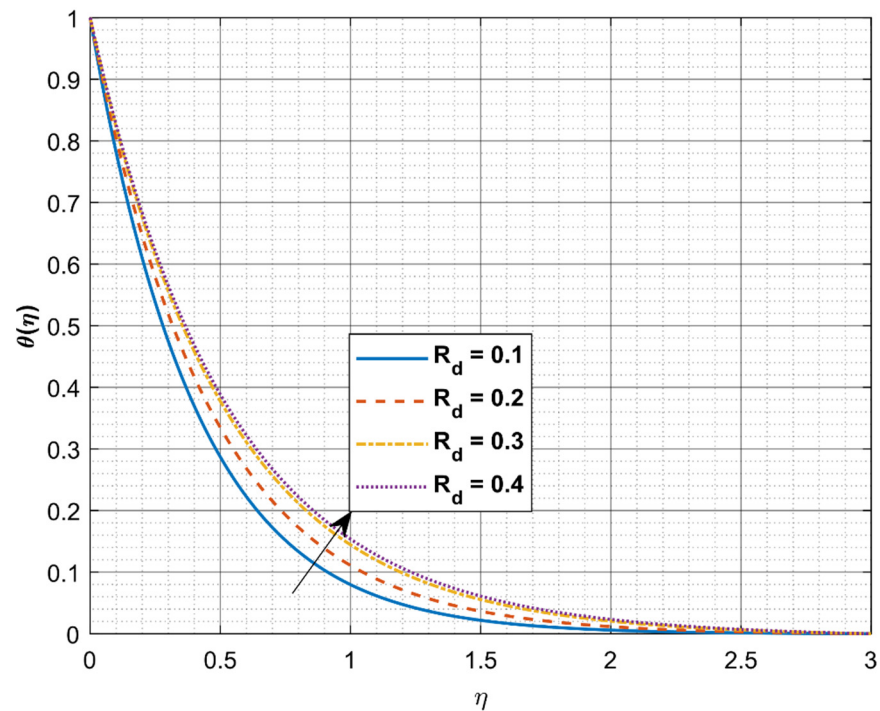


Figure 9. Influence of  $R_d$  on  $\theta(\eta)$ .

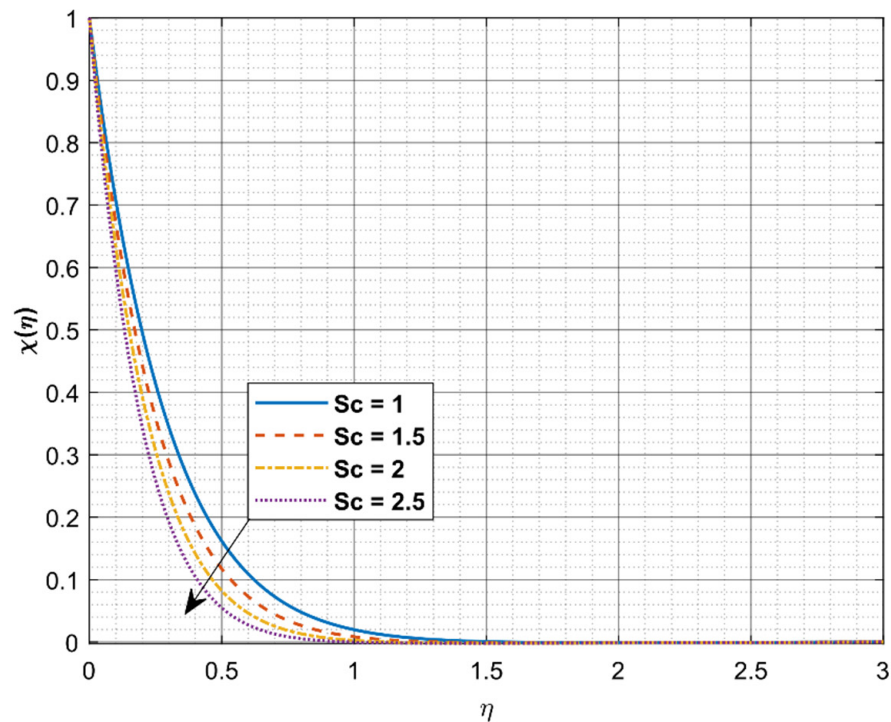
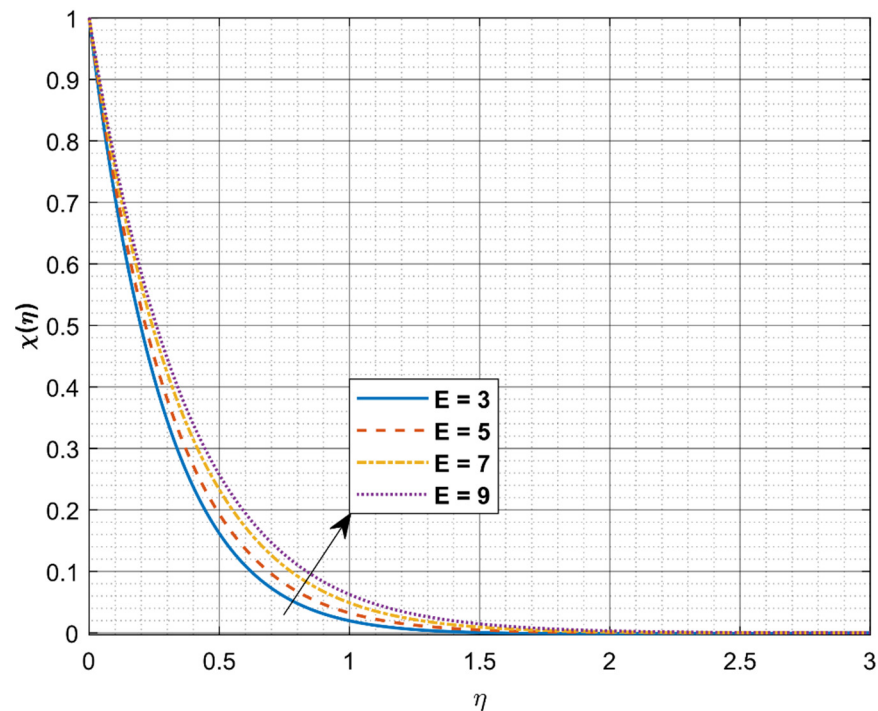


Figure 10. Influence of  $Sc$  on  $\chi(\eta)$ .

We note that most parameters have little effect on velocity or temperature, so we turn our attention to parameters related to activation energy. The effect of  $E$  on mass transfer is shown in Figure 11. Here, an increase in  $E$  improves the concentration gradient. Mathematically, the Arrhenius equation describes the introduction of activation energy into any system, which explicitly shows that the reduction in the heat and acceleration results in a low reaction rate constant. This causes the chemical reaction to slow down, resulting in a greater particle concentration. As the activation energy  $E$  becomes larger, the

modified Arrhenius mechanism decays. This ultimately stimulates the generative chemical reaction, which causes the concentration of nanoparticles to increase.



**Figure 11.** Influence of  $E$  on  $\chi(\eta)$ .

In fluid mechanics, the Nusselt number is the ratio of convective to conductive heat flow at a fluid's boundary. Figure 12 displays the effect of  $\alpha_2$  and  $\lambda^*$  on  $Nu$ . Finally, the Nusselt number is found to decrease as  $\lambda^*$  increases. This is in line with the fact that increasing  $\lambda^*$  adds some extra tension which is responsible for an increase in the heat transfer rate. Figure 13 shows the effect of  $M$  and  $R_d$  on  $Nu$ . Here, as the value of  $M$  is increased, the heat transfer rate is reduced. Furthermore, the Nusselt number is found to decrease as a function of  $R_d$ . The increasing value of  $R_d$  causes the material particles to have more kinetic energy, which increases the thermal field. As a result, the radiative variable would result in a greater thermal field. Figures 14–16 represent the streamlines of the flow pattern. The stream function simply ascends into the boundary layer as distance increases. Generally, streamlines are the paths of imaginary particles suspended in a liquid that are transported along with it. The fluid speed is relatively high when streamlines clump together; the fluid speed is relatively low where they open out.

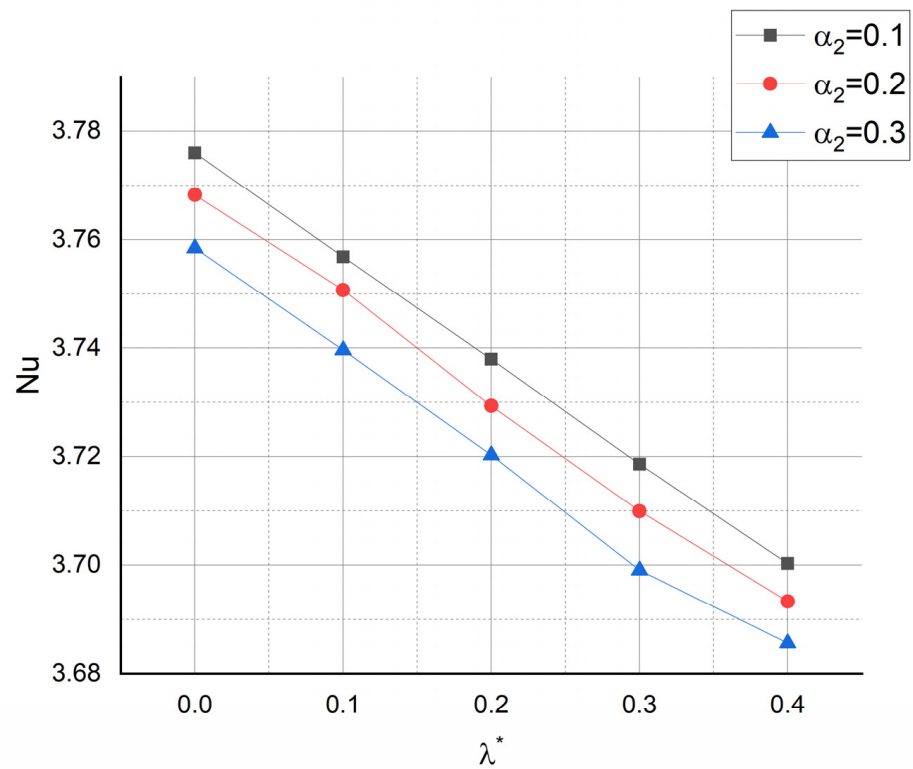


Figure 12. Influence of  $\alpha_2$  and  $\lambda^*$  on  $Nu$ .

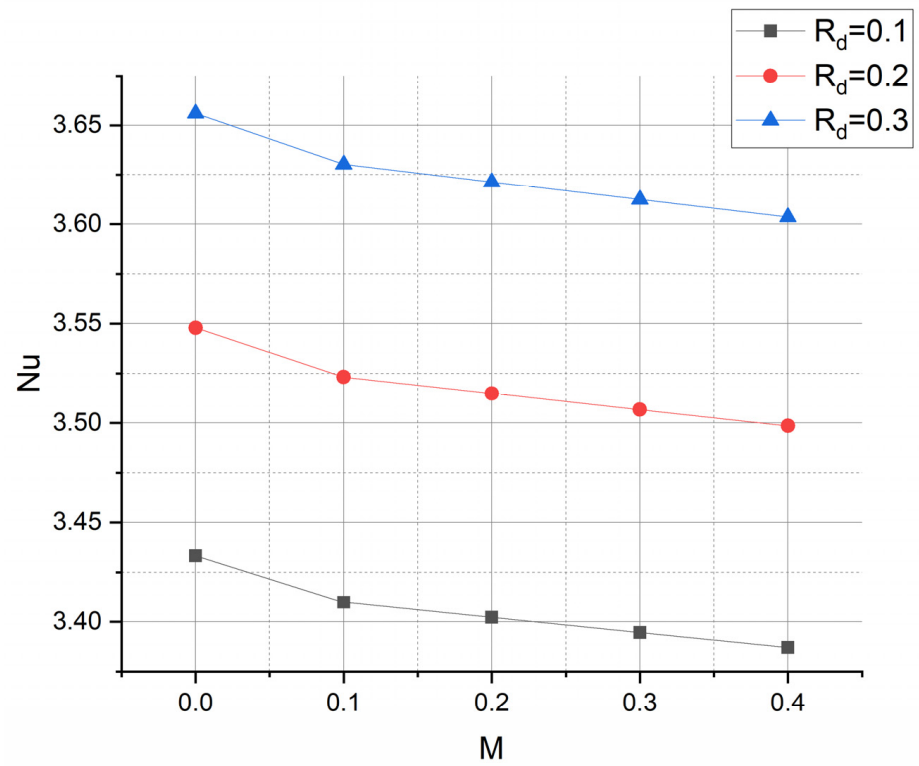


Figure 13. Influence of  $M$  and  $R_d$  on  $Nu$ .

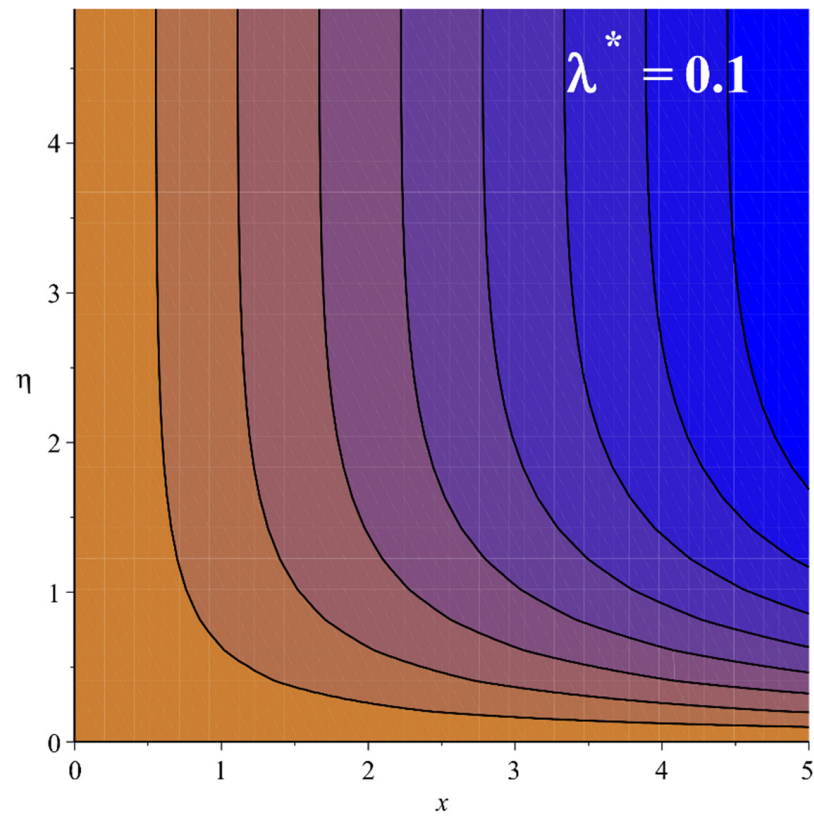


Figure 14. Stream lines when  $\lambda^* = 0.1$ .

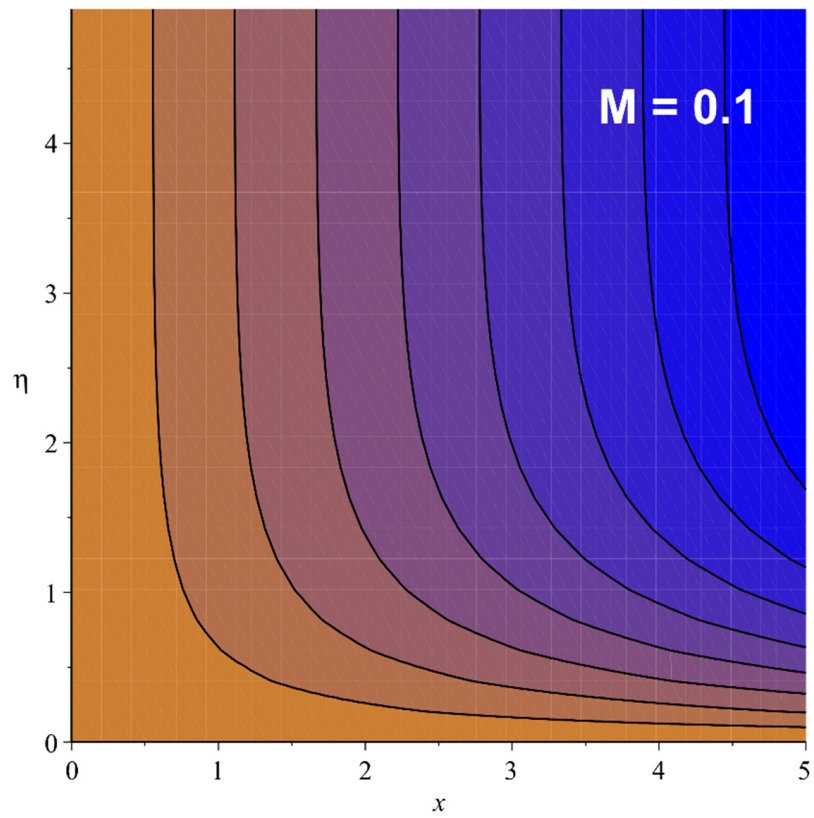
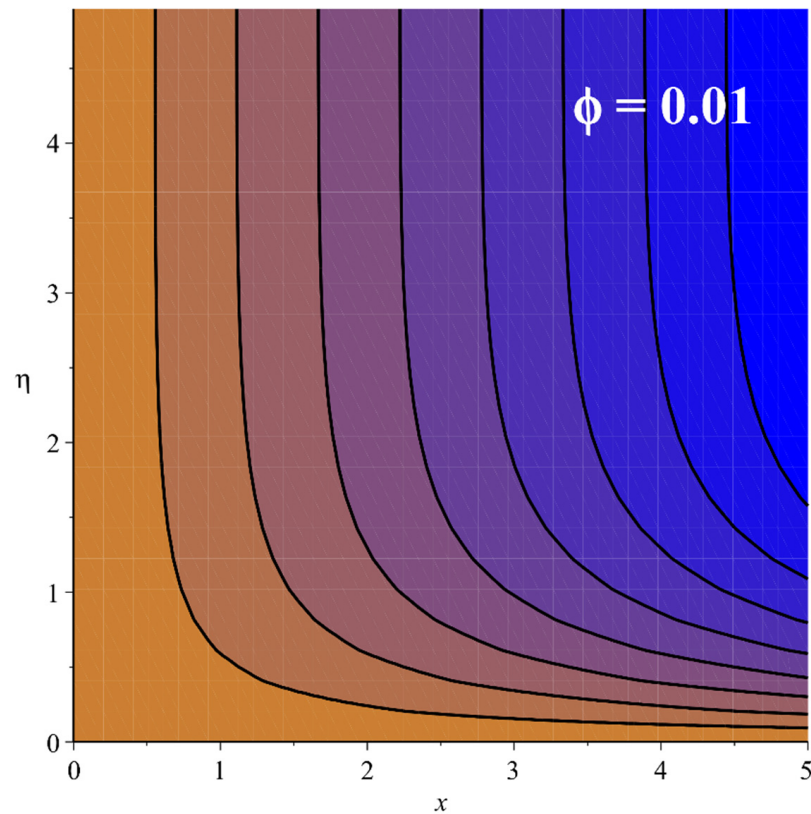


Figure 15. Stream lines when  $M = 0.1$ .



**Figure 16.** Stream lines when  $\phi = 0.01$ .

## 6. Final Remarks

In this investigation, we studied the Marangoni convection, magnetic and thermal radiation effects on second-grade nanofluid flow over a surface in the presence of a permeable medium and a uniform heat sink/source. The non-Newtonian nanofluid suspended with  $TC_4$  as nanoparticles in base fluid engine oil (unused) is utilized in this modelling. Using similarity transformations, the resulting equations for momentum, concentration and energy were transformed into ODEs. These equations are numerically solved via RKF-45 method. The solutions of velocity, temperature and concentration fields are presented for several parameters of the flow. The main results of the present examination are as follows:

- The increasing values of the Marangoni number improve the velocity gradient and declines the heat transfer;
- The increasing values of the magnetic parameter improve the velocity gradient and declines the heat transfer;
- The rising values of radiation and heat source/sink parameters improve the heat transfer;
- The boost-up values of porosity parameter decay the velocity gradient and improve the heat transfer;
- The enhancement in the Schmidt number declines the concentration gradient;
- The increase in the activation energy parameter improves the concentration gradient;
- The increasing values of second-grade and porosity parameters declines the heat transfer rate.

It is essential to study how to develop correlations of heat, flow and mass transfer characteristics for hybrid nanofluid, as well as nanofluid, considering various nanoparticles. Therefore, upcoming works could be associated with the study of entropy generation along with the effect of thermal radiation, as well as nanofluid flow in porous media containing microorganisms, to develop a numerical model considering mass transfer contributions in non-Newtonian nanofluid flow, employing the two-phase model for nanofluids to

develop well-focused numerical models and to simulate different types of thermal and hydrodynamics boundary conditions and geometries (e.g., flat, elliptical or circular).

**Author Contributions:** Conceptualization, B.C.P. and I.E.S.; methodology, B.C.P.; software, R.J.P.G.; validation, R.N.K., B.C.P.; formal analysis, I.E.S.; investigation A.M.J.; resources, B.C.P.; data curation, I.E.S.; writing—original draft preparation, I.E.S.; writing—review and editing, B.C.P. and I.E.S.; visualization, B.C.P.; supervision, B.C.P.; project administration, B.C.P. All authors have read and agreed to the published version of the manuscript.

**Funding:** This research received no external funding.

**Institutional Review Board Statement:** Not applicable.

**Informed Consent Statement:** Not applicable.

**Conflicts of Interest:** The authors declare no conflict of interest.

## Nomenclature

$(u : v)$	Fluid phase velocity along the x, y-direction.	$\eta$	Similarity variable
$\rho$	Density	$T$	Temperature
$\gamma_T$	Rate of change of surface tension with respect to fluid temperature	$\lambda^*$	Porosity parameter
$M$	Magnetic parameter	$Q_0$	Heat sink/source parameter
$\nu$	Kinematic viscosity	$\alpha_1$	Material-related parameter
$R_d$	Radiation parameter	$Q$	Heat source/sink coefficient
$k^*$	Boltzmann constant	$Pr$	Prandtl number
$K^*$	Porous medium permeability	$\alpha_2$	Second grade parameter
$D$	Diffusion coefficient	$Nu$	Nusselt number
$\sigma^*$	Chemical reaction rate parameter	$Sc$	Schmidt number
$B_0$	Magnetic field	$\sigma_1$	Electrical conductivity
$m$	Fitted rate constant	$E_a$	Activation energy
$\mu$	Dynamic viscosity	$\delta$	Temperature difference
$\sigma_0$	Surface tension at the interface	$k$	Thermal conductivity
$E$	Dimensionless activation energy	Subscript	
$Ma$	Marangoni number	f	fluid
$L$	Reference length	nf	nanofluid
$k_r^2$	Reaction rate	w	Wall/surface
$\sigma$	Surface tension	$\infty$	ambient

## References

- Hayat, T.; Iqbal, Z.; Mustafa, M. Flow of a Second Grade Fluid over a Stretching Surface with Newtonian Heating. *J. Mech.* **2012**, *28*, 209–216. [\[CrossRef\]](#)
- Javanmard, M.; Taheri, M.H.; Abbasi, M. Analytical and Numerical Investigation of Second Grade Magneto-hydrodynamics Flow over a Permeable Stretching Sheet. *J. Comput. Appl. Mech.* **2020**, *51*, 239–246. [\[CrossRef\]](#)
- Hayat, T.; Khan, W.A.; Abbas, S.Z.; Nadeem, S.; Ahmad, S. Impact of induced magnetic field on second-grade nanofluid flow past a convectively heated stretching sheet. *Appl. Nanosci.* **2020**, *10*, 3001–3009. [\[CrossRef\]](#)
- Krishna, M.V.; Jyothi, K.; Chamkha, A.J. Heat and mass transfer on mhd flow of second-grade fluid through porous medium over a semi-infinite vertical stretching sheet. *J. Porous Media* **2020**, *23*, 751–765. [\[CrossRef\]](#)
- Kalaivanan, R.; Ganesh, N.V.; Al-Mdallal, Q.M. An investigation on Arrhenius activation energy of second grade nanofluid flow with active and passive control of nanomaterials. *Case Stud. Therm. Eng.* **2020**, *22*, 100774. [\[CrossRef\]](#)
- Choi, S. Enhancing Thermal Conductivity of Fluids with Nanoparticles. *Am. Soc. Mech. Eng. Fluids Eng. Div. Publ. FED* **1995**, *231*, 99–105.
- Radhika, M.; Gowda, R.J.P.; Naveenkumar, R.; Siddabasappa; Prasannakumara, B.C. Heat transfer in dusty fluid with suspended hybrid nanoparticles over a melting surface. *Heat Transf.* **2021**, *50*, 2150–2167. [\[CrossRef\]](#)
- Shafiq, A.; Rasool, G.; Khalique, C.M.; Aslam, S. Second Grade Bioconvective Nanofluid Flow with Buoyancy Effect and Chemical Reaction. *Symmetry* **2020**, *12*, 621. [\[CrossRef\]](#)
- Shah, Z.; Alzahrani, E.O.; Dawar, A.; Alghamdi, W.; Ullah, M.Z. Entropy Generation in MHD Second-Grade Nanofluid Thin Film Flow Containing CNTs with Cattaneo-Christov Heat Flux Model Past an Unsteady Stretching Sheet. *Appl. Sci.* **2020**, *10*, 2720. [\[CrossRef\]](#)

10. Gowda, R.P.; Kumar, R.N.; Aldalbahi, A.; Issakhov, A.; Prasannakumara, B.; Rahimi-Gorji, M.; Rahaman, M. Thermophoretic particle deposition in time-dependent flow of hybrid nanofluid over rotating and vertically upward/downward moving disk. *Surfaces Interfaces* **2021**, *22*, 100864. [[CrossRef](#)]
11. Bestman, A.R. Natural convection boundary layer with suction and mass transfer in a porous medium. *Int. J. Energy Res.* **1990**, *14*, 389–396. [[CrossRef](#)]
12. Khan, N.S.; Kumam, P.; Thounthong, P. Second law analysis with effects of Arrhenius activation energy and binary chemical reaction on nanofluid flow. *Sci. Rep.* **2020**, *10*, 1–16. [[CrossRef](#)] [[PubMed](#)]
13. Jayadevamurthy, P.G.R.; Rangaswamy, N.K.; Prasannakumara, B.C.; Nisar, K.S. Emphasis on unsteady dynamics of bioconvective hybrid nanofluid flow over an upward–downward moving rotating disk. *Numer. Methods Partial. Differ. Equ.* **2020**. [[CrossRef](#)]
14. Reddy, M.G.; Naveen, K.R.; Prasannakumara, B.; Rudraswamy, N.G.; Kumar, K.G. Magnetohydrodynamic flow and heat transfer of a hybrid nanofluid over a rotating disk by considering Arrhenius energy. *Commun. Theor. Phys.* **2021**, *73*, 045002. [[CrossRef](#)]
15. Zhao, H.; Zhang, Y.; Liu, P.; Yap, P.; Ser, W.; Liu, A. Chemical reaction monitoring via the light focusing in optofluidic waveguides. *Sens. Actuators B Chem.* **2019**, *280*, 16–23. [[CrossRef](#)]
16. Rasool, G.; Zhang, T.; Shafiq, A. Marangoni Effect in Second Grade Forced Convective Flow of Water Based Nanofluid. *J. Adv. Nanotechnol.* **2018**, *1*, 50–61. [[CrossRef](#)]
17. Khan, S.A.; Hayat, T.; Alsaedi, A.; Zai, Q.M.Z. Irreversibility analysis in Marangoni forced convection flow of second grade fluid. *J. Phys. Commun.* **2020**, *4*, 085013. [[CrossRef](#)]
18. Hayat, T.; Khan, S.A.; Alsaedi, A.; Fardoun, H.M. Marangoni Forced Convective Flow of Second Grade Fluid with Irreversibility Analysis and Chemical Reaction. *Int. J. Thermophys.* **2021**, *42*, 1–21. [[CrossRef](#)]
19. Ullah, I.; Hayat, T.; Alsaedi, A.; Asghar, S. Modeling for radiated Marangoni convection flow of magneto-nanoliquid subject to Activation energy and chemical reaction. *Sci. Iran.* **2020**, *27*, 3390–3398. [[CrossRef](#)]
20. Qayyum, S. Dynamics of Marangoni convection in hybrid nanofluid flow submerged in ethylene glycol and water base fluids. *Int. Commun. Heat Mass Transf.* **2020**, *119*, 104962. [[CrossRef](#)]
21. Hayat, T.; Aziz, A.; Muhammad, T.; Ahmad, B. On magnetohydrodynamic flow of second grade nanofluid over a nonlinear stretching sheet. *J. Magn. Magn. Mater.* **2016**, *408*, 99–106. [[CrossRef](#)]
22. Sajid, M.; Hayat, T. Influence of thermal radiation on the boundary layer flow due to an exponentially stretching sheet. *Int. Commun. Heat Mass Transf.* **2008**, *35*, 347–356. [[CrossRef](#)]
23. Kandasamy, R.; Mohamad, R.; Ismoen, M. Impact of chemical reaction on Cu, Al<sub>2</sub>O<sub>3</sub> and SWCNTs–nanofluid flow under slip conditions. *Eng. Sci. Technol. Int. J.* **2016**, *19*, 700–709. [[CrossRef](#)]
24. Tlili, I.; Sandeep, N.; Reddy, M.G.; Nabwey, H.A. Effect of radiation on engine oil-TC4/NiCr mixture nanofluid flow over a revolving cone in mutable permeable medium. *Ain Shams Eng. J.* **2020**, *11*, 1255–1263. [[CrossRef](#)]
25. Mabood, F.; Shateyi, S. Multiple Slip Effects on MHD Unsteady Flow Heat and Mass Transfer Impinging on Permeable Stretching Sheet with Radiation. *Model. Simul. Eng.* **2019**, *2019*, 3052790. [[CrossRef](#)]
26. Pal, D. Combined effects of non-uniform heat source/sink and thermal radiation on heat transfer over an unsteady stretching permeable surface. *Commun. Nonlinear Sci. Numer. Simul.* **2011**, *16*, 1890–1904. [[CrossRef](#)]
27. Haile, E.; Shankar, B. Heat and Mass Transfer in the Boundary Layer of Unsteady Viscous Nanofluid along a Vertical Stretching Sheet. *J. Comput. Eng.* **2014**, *2014*, 345153. [[CrossRef](#)]
28. Ishak, A.; Nazar, R.; Pop, I. Boundary layer flow and heat transfer over an unsteady stretching vertical surface. *Meccanica* **2008**, *44*, 369–375. [[CrossRef](#)]
29. Ali, B.; Yu, X.; Sadiq, M.T.; Rehman, A.U.; Ali, L. A Finite Element Simulation of the Active and Passive Controls of the MHD Effect on an Axisymmetric Nanofluid Flow with Thermo-Diffusion over a Radially Stretched Sheet. *Processes* **2020**, *8*, 207. [[CrossRef](#)]